Clonal analysis reveals nerve-dependent and independent roles on mammalian hind limb tissue maintenance and regeneration

Yuval Rinkevich[a,1,2], Daniel T. Montoro[b,1,2], Ethan Muhonen[b,1], Graham G. Walmsley[a,b], David Lo[b], Masakazu Hasegawa[b], Michael Januszyk[b], Andrew J. Connolly[c], Irving L. Weissman[a,2], and Michael T. Longaker[a,b,2]

[a]Institute for Stem Cell Biology and Regenerative Medicine, Department of Pathology, and Department of Developmental Biology, [b]Hagey Laboratory for Pediatric Regenerative Medicine, Department of Surgery, Plastic and Reconstructive Surgery, and [c]Department of Pathology, Stanford University School of Medicine, Stanford, CA 94305

Contributed by Irving L. Weissman, June 1, 2014 (sent for review January 14, 2014)

The requirement and influence of the peripheral nervous system on tissue replacement in mammalian appendages remain largely undefined. To explore this question, we have performed genetic lineage tracing and clonal analysis of individual cells of mouse hind limb tissues devoid of nerve supply during regeneration of the digit tip, normal maintenance, and cutaneous wound healing. We show that cellular turnover, replacement, and cellular differentiation from presumed tissue stem/progenitor cells within hind limb tissues remain largely intact independent of nerve and nerve-derived factors. However, regenerated digit tips in the absence of nerves displayed patterning defects in bone and nail matrix. These nerve-dependent phenotypes mimic clinical observations of patients with nerve damage resulting from spinal cord injury and are of significant interest for translational medicine aimed at understanding the effects of nerves on etiologies of human injury.

pattern formation | peripheral nerve | stem cell

The regrowth of vertebrate appendages has been considered a classic model system for interrogating the mechanisms and requirements for tissue/organ generation and regeneration across various phyla (1–5). Urodeles regenerate entire limbs by proliferation of fate-restricted stem and progenitor cells and form a blastema, the collection of cells at the interface of stump and wound epidermis, in a process mediated by nerve-derived factors (6–10). In Urodeles, surgical denervation before amputation results in the inhibition of blastema formation, and ultimately results in regeneration failure. Evidence from fish and amphibians suggests that nerve dependence may be a function of a threshold level of nerve factors with a direct correlation between nerve fibers and degree of regeneration (3, 11, 12) and supports the idea that nerve dependence may be an evolutionarily conserved requirement for the regeneration of vertebrate limb tissues.

Mammalian limbs consist of multiple tissues that are derived from various embryonic origins and germ layers, including embryonic ectoderm, embryonic mesoderm, and embryonic neural-crest. Recent lineage-tracing studies have demonstrated that tissue-resident stem and progenitor cells that are fate-restricted in their developmental potential are responsible for appendage regeneration of fish, salamanders, and mice (13–16). These cumulative data demonstrate that fate-restricted stem/progenitors as cells of origin, rather than dedifferentiation or transdifferentiation of terminally differentiated cells, represents an evolutionarily conserved cellular mechanism that explains the observed regrowth of the vertebrate appendages.

Collectively, the commonalities of nerve dependence and stem/progenitor fate restriction across vertebrate phyla further highlight the possibility that nerve dependence on appendage regrowth may take place within mammals, and possibly humans. In support of this, human clinical reports indicate that skin complications are manifested in response to spinal cord injury (SCI), suggesting a role of the nervous system in the maintenance of skin and nail organ. For example, histopathology studies report SCI patients presenting with dermal fibrosis, progressive skin thickening, and nail hypertrophy on lower limbs/digits after SCI (17, 18). The severity of the phenotypes in these studies is progressive and directly correlated with the degree of injury.

To directly interrogate the peripheral nerve requirements of mammalian hind limb tissues, we used a novel transgenic line that permits in vivo clonal analysis of individual cells to describe the clonal read-out of primary limb tissues in response to denervation during maintenance, regeneration, and cutaneous wound healing. Earlier studies in mice have indicated there is some evidence for replacement of the mouse digit tip after sciatic denervation but did not directly examine tissue or cellular outcomes (19). A recent study has reopened a similar line of inquiry and reports that surgical denervation before digit tip amputation results in the suppression of blastema growth, potentially by the attenuation of Wnt signaling in distal nail epithelium (20).

In this study, we directly and comprehensively examine several primary tissues that are normally innervated during conditions of maintenance, regeneration, and dermal wound healing. We show that many of the tissue resident stem/progenitor cells undergo continuous renewal and differentiation, despite the absence of peripheral nerves, but with patterning phenotypes in both nail and bone. These observations correlate with human clinical reports in SCI patients and have significant implications for basic and translational research aimed at the etiology and amelioration of nerve-dependent limb pathologies.

Significance

In Urodeles, surgical denervation before limb amputation results in regeneration failure. Here we explored the dependency of the peripheral nervous system on tissue replacement in mammalian appendages by performing a comprehensive clonal analysis of hind limb tissues devoid of nerve supply. Our experiments uncover conserved phenotypes, which mimic clinical observations of patients with nerve damage resulting from spinal cord injury. Our system could be used to better understand both pathophysiology and treatment of patients with spinal cord injury.

Author contributions: Y.R., D.T.M., and M.T.L. designed research; Y.R., D.T.M., D.L., and M.H. performed research; Y.R., D.T.M., E.M., G.G.W., M.J., and A.J.C. analyzed data; M.J. performed statistical analysis; A.J.C. performed morphometric analysis; and Y.R., D.T.M., I.L.W., and M.T.L. wrote the paper.

The authors declare no conflict of interest.

[1]Y.R., D.T.M., and E.M. contributed equally to this work.

[2]To whom correspondence may be addressed. E-mail: ryuval@stanford.edu, danmontoro@gmail.com, irv@stanford.edu, or longaker@stanford.edu.

This article contains supporting information online at www.pnas.org/lookup/suppl/doi:10.1073/pnas.1410097111/-/DCSupplemental.

Results

Chronic denervation was accomplished by surgically removing 0.5 cm of the sciatic and femoral nerves with cauterizing dipoles. Transection of the sciatic nerve (Fig. S1*A*, arrow) disrupted sensory nerve supply to the entire distal limb and skin covering the posterior thigh and gluteal regions, whereas transection of the femoral nerve (Fig. S1*B*, arrow) disrupted anterior cutaneous and muscular branches in the thigh, as well as quadriceps femoris muscle and articular branches to the knee joint. As a control for off-target effects of the procedure, sham control surgeries were performed on the contralateral limb tissues and revealed beta III tubulin immunoreactivity in epidermis, hair follicles (Fig. S1*C*), and sweat glands (Fig. S1*D*). Absence of innervation was confirmed after denervation by a progressive reduction in immunoreactivity of pan-neuronal marker beta III tubulin after 2 wk (Fig. S1 *E* and *F*) and 3 mo (Fig. S1 *G* and *H*) in epidermis, hair follicles, and sweat glands. On the basis of these results, clonal tracing was initiated by tamoxifen administration to the experimental and sham-control mice 2 wk postsurgery, so as not to include cellular expansions that may have resulted from the activity of nerve remnants or dying peripheral nerves before their complete degeneration.

To trace individual cells of all hind limb tissues in vivo over long periods of time, we performed the denervation procedures in rainbow reporter ($R26^{VT2/GK3}$) mice; a multicolor Cre-dependent marker system that harbors a four-color (green, blue, yellow, red) reporter construct within the *ROSA* locus. After recombination, each cell is randomly and permanently (genetically) marked with one of four colors, resulting in a mosaic fluorescent pattern within tissues. Daughter cells maintain the same color as the cell of origin, such that products of clonal divisions can be visualized as expanding regions of a single color. Rainbow mice were crossed with the ubiquitous $Actin^{CreER}$ driver so as to universally mark, and clonally trace, all cells within hind limb tissues after administration of tamoxifen. This approach permits a more comprehensive clonal readout of cells, including rare stem cells, as opposed to using tissue-specific or stem cell-specific reporters such as SRY(sex determining region Y)-box gene 9, Cytokeratin 15, or leucine-rich G protein-coupled receptor 5 for hair follicle stem cells (21). Thus, labeling is independent of a change in marker gene expression that could occur after denervation. Despite the chance of two adjacent cells being similarly colored, we and others (16, 22, 23) have found that lineage tracing over long periods of time uncovers a faithful cellular readout to that observed using tissue-specific or stem cell-specific reporters. Furthermore, as this assay can be used broadly to trace all cell types, it allows clonal analysis of even rare and as-yet-unidentified tissue stem cells that may be activated on denervation and that would not be uncovered using existing stem cell reporters.

Nerve Dependence on Hind Limb Tissue Maintenance. Tissue homeostasis is a process mediated by the self-renewal and differentiation of tissue-resident stem/progenitors (24, 25). We therefore analyzed the effects of sciatic and femoral nerve denervation on the proliferation and differentiation capacities of proximal, medial, and distal hind limb tissues. First, we analyzed the clonal patterns that emerged within the epidermis and its associated appendages during 3 mo posttamoxifen administration.

Ventral epidermis of the paw and hind limbs (proximal to eccrine sweat glands) showed continuous turnover accompanied by self renewal and differentiation of $K14^+$ basal keratinocytes in control (mean cells/clone, 5.5; range of cells/clone, 1–18; $n = 38$; Fig. 1*A*) and denervated (mean cells/clone, 4.68; range of cells/clone, 1–19; $n = 74$; Fig. 1*B*) hind limbs.

Ventral eccrine sweat glands appeared largely polyclonal, with multiple cells per clone in control (mean cells/clone, 3.12; range of cells/clone, 1–6; $n = 25$) and denervated (mean cells/clone, 2.73; range of cells/clone, 1–6; $n = 62$) limbs. Cellular expansion

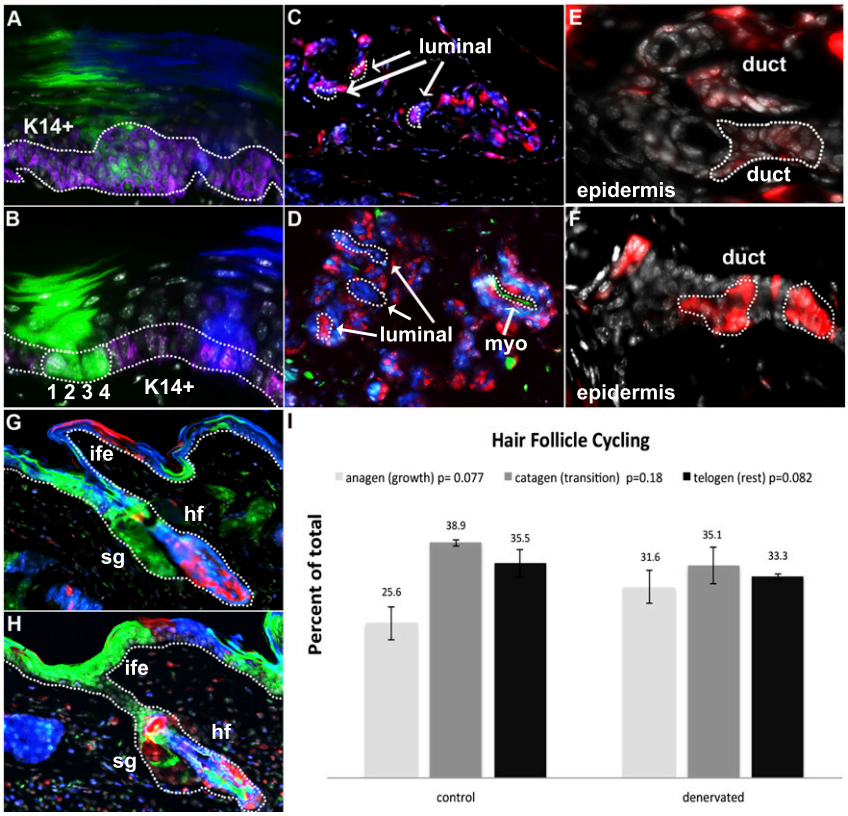

Fig. 1. Clonal maintenance of epidermal appendages. $K14^+$ basal keratinocyte clones (purple) self-renew within the keratinocyte layer in control (*A*) and denervated (*B*) epidermis of the hind limb and differentiate into corneal layers of epidermis. 1, 2, 3, and 4 indicate numeral values of single $K14^+$ basal keratinocytes in a single clone. Sweat glands are populated by small clones in myoepithelial and luminal cells, indicating slow continuous replacement in control (*C*) and denervated (*D*) glands. Sweat ducts bridging sweat gland and epidermis display similar clonal expansion within duct structures, indicating intrinsic self-renewal capabilities of control (*E*) and denervated (*F*) ducts. Clones populate hair follicle (hf) bulge, sebaceous gland (sg), and interfollicular epidermal (ife) regions within control (*G*) and denervated (*H*) limbs but are not observed to span multiple regions. Proportions of hair follicle populations in anagen (growth), catagen (transition), and telogen (rest) phases (*I*) in control and denervated limbs show statistically similar proportions of hair follicles in each phase in the absence of nerves.

and tissue renewal took place in both myoepithelial and luminal secreting portions of eccrine sweat glands in control (Fig. 1*C*) and denervated (Fig. 1*D*) hind paws. Single clones were not observed to span both myoepithelial and luminal secreting portions, suggesting that stem/progenitor specificity or restriction between these cell types is maintained during homeostatic replacement and is independent of nerve supply.

Sweat gland ducts revealed clones in both control (Fig. 1*E*) and denervated (Fig. 1*F*) hind limbs, indicating that progenitors in ductal regions continuously contribute to sweat gland duct renewal in a process independent of nerve supply. Single clones were not observed to significantly span underlying epidermis, adjacent keratinocyte layers, or the myoepithelial or luminal cells of the sweat gland, suggesting specificity to duct structures is similarly unaffected by the lack of nerve supply.

During our 3-mo tracing period, significant tissue renewal occurred within the hair follicle bulge, sebaceous gland, and interfollicular epidermal regions in both control (mean cells/clone, 6.07; range of cells/clone, 1–23; $n = 72$) and denervated (mean cells/clone, 6.25; range of cells/clone, 1–27; $n = 104$) hair follicles of the hind limb. Regional restriction of clones to hair follicle, sebaceous gland, or interfollicular epidermal was observed in control (Fig. 1*G*) and denervated (Fig. 1*H*) samples, with the absence of clones that spanned beyond a single epidermal region indicating that developmental potential and regional specificity of epidermal stem cells is independent of nerves.

Having shown that denervation did not inhibit stem/progenitor self-renewal and differentiation within the epidermis and epidermal appendages, we then examined whether denervation affects hair cycle progression. Within denervated hind limb, we found statistically similar proportions of hair follicles in each phase of hair cycle progression compared with the control limb ($n_{control} = 288$, $n_{denervated} = 268$, $p_{anagen} = 0.077$, $n_{anagen} = 87$, $p_{catagen} = 0.18$, $n_{catagen} = 111$, $p_{telogen} = 0.082$, $n_{telogen} = 109$) (Fig. 1*I*), with consistent results in each individual animal (Fig. S2 *A* and *B*).

Tissues of long bones, including their marrow cavity, undergo constant maintenance and renewal (26). We therefore examined the long bones for differences in either bone shape or thickness. Histological examinations of control and denervated hind limb tibia and fibula showed no obvious morphologic or histologic differences in either bone shape or thickness, nor structural abnormalities of marrow cavities (observations by A.J.C.) Within articular cartilage, we found multiple clones of chondrocytes ranging from 3 to 6 cells per clone in both control (Fig. 2*A*) and denervated (Fig. 2*B*) joints, suggesting tissue maintenance by long bones is independent of nerve supply.

Tendons are also innervated tissues (27) and were examined in this study for nerve dependence. Within the mouse flexor digitorum tendons, which run along the inferior side of the phalanges, we found large clones of up to 10 cells throughout the width of and at the edges of tendons (Fig. 2*C*). Similar patterns were observed in both denervated limbs (Fig. 2*D*), indicating that despite the close association between tendons and nerve endings, the renewal of tenocytes does not depend on stimulation from nerves in vivo.

Nerve Dependence on Hind Limb Digit Regeneration. To analyze the contributions of nerves to murine digit regeneration, digit amputations were performed 2 wk postdenervation on the middle three digits of denervated ($n = 12$) and sham control ($n = 12$) hind limb digits along an amputation plane that removed portions of the distal phalange bone, nail organ, and sweat glands (16). Three months postamputation, digits were collected and processed for histological and clonal analysis, distal from sites of amputation (Fig. S3). We first examined whether denervated nerves would regenerate during the 3-mo tracing period, which would confound our conclusions. In normal digit tips ($n = 12$), the epidermis and hair follicles on the dorsal side contain sensory

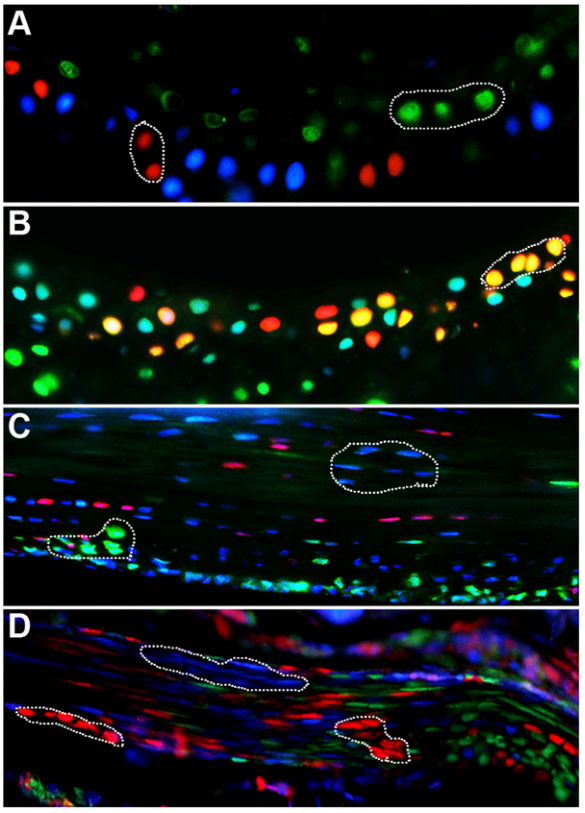

Fig. 2. Clonal maintenance in mesoderm-derived limb tissues. Clones within isogenous groups of articular cartilage indicate continuous proliferations in control (*A*) and denervated (*B*) hyaline cartilage. Clonal expansions of tenocytes inside and along the edge of the tendon in control (*C*) and denervated (*D*) flexor tendon suggests continuous cell division.

innervations, whereas sweat glands on the ventral side are innervated by sympathetic nerves, which have been previously shown to be necessary for sweat gland maturation during limb development (28, 29). Consistent with these reports, control digits showed robust label of beta III tubulin in epidermal appendages (Fig. S1 *C* and *D*), suggesting they may be prone to nerve dependence. Staining of epidermal appendages at 2 wk (Fig. S1 *E* and *F*) and 3 mo (Fig. S1 *G* and H) postamputation showed minimal beta III tubulin label in the denervated tissues compared with control tissues, indicating that regeneration of peripheral hind limb nerves that follow denervation does not occur during the 3-mo time course of digit tip regeneration.

Regenerated ventral epidermis at the distal digit tip showed keratinocyte duplications in the basal layers and differentiation into flat cornified layers in the control (Fig. 3*A*; mean cells/clone, 7.86; range of cells/clone, 1–32; $n = 35$) and denervated (Fig. 3*B*; mean cells/clone, 7.34; range of cells/clone, 1–32; $n = 85$) groups.

Eccrine sweat glands within the regenerated region of the digit tip showed similar clonal trends between control (Fig. 3*C*; mean cells/clone, 2.14; range of cells/clone, 1–9, $n = 167$) and denervated (Fig. 3*D*; mean cells/clone, 1.91; range of cells/clone, 1–12; $n = 134$) groups, with separate clones contributing to myoepithelial and luminal secreting cell populations. A similar clonal pattern was observed in eccrine sweat glands within more proximal regions of the ventral paw, in which there was absence of clones containing both myoepithelial and luminal secreting cells (observations by D.T.M). Moreover, eccrine sweat glands within denervated digits ($n = 12$) regenerated whole duct structures that reached the ventral epidermal surface but that did not contribute to myoepithelial or luminal secreting cells, consistent with recent publications

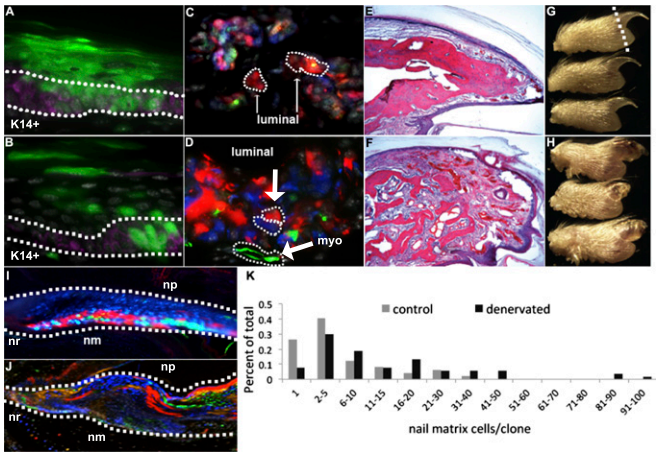

Fig. 3. Regeneration of digit tips after amputation. Control (*A*) and denervated (*B*) digits show that keratinocytes (marked by K14 expression in purple) regenerate after amputation and undergo self renewal within the basal layer (outlined by a dotted line in *B*) and differentiation (into cornified layers) of epidermis. Control (*C*) and denervated (*D*) digits show sweat glands regenerate and display independent clones within luminal and myoepithelial cell types (dotted lines in *D* indicate separate clones). Both control (*E*) and denervated (*F*) digits regenerate the amputated portion of the distal phalanx via direct ossification, although the denervated replacement bone lacks a distinct trabecular organization. Gross morphology of regenerated control (*G*) digit tips and regenerated and denervated (*H*) digit tips with patterning defects. Dotted line in *G* indicates plane of amputation. Nail root (nr) and matrix (nm) populate the nail organ with large dominant clones during regeneration of the control (*I*) and denervated (*J*) nail organ. Denervated nail matrix clones demonstrate a right shift in the distribution of the number of cells contained within a single clone compared with control nail matrix clones (*K*).

describing separate myoepithelial, luminal, and ductal progenitors within sweat glands (16, 30).

Distal to the site of amputation, we saw significant regeneration of bone via direct ossification of osteoblast-like cells that arranged along the surface of de novo osteoid in both control (Fig. 3*E*) and denervated (Fig. 3*F*) digit tips, consistent with previous reports (19). The replacement bone of the sham control distal phalanx appeared structurally similar to a nonamputated phalanx (Fig. 3*E*); however, in marked contrast, the phalanx of denervated digits failed to pattern into the typical trabecular arrangement (Fig. 3*F*), with histological abundant loose connective tissue and dense bundles of vascularization. Gross morphology indicated that these nerve-dependant patterning defects have been extended to the regenerating nail organ (cf. Fig. 3 *G* and *H*). Morphometric analysis (see *Experimental Procedures*) indicated that the outer contours of the regenerated distal phalanges from control mice achieved a natural taper (0.54 ± 0.10), whereas the denervated mice lacked taper (0.09 ± 0.13). Moreover, control digits had cortical bone covered by periosteum over most of their surface (86 ± 23%), whereas the denervated mice had very little cortical bone on their surface (13 ± 17%) and consisted mostly of irregular callus-type trabeculae surround by osteoblasts, osteoclasts, and reactive stroma. Finally, denervated digits exhibited more active fibroblastic/mesenchymal proliferation and vascularity in the distal soft tissues beyond the callus-like bone, which was confluent with the stroma extending between the healing woven bone.

We found large clonal regions that spanned the nail root and nail matrix in both control (Fig. 3*I*) and denervated (Fig. 3*J*) nail organs. However, the clones of the control nail organ (mean cells/clone, 6.78; range of cells/clone, 1–41; $n = 49$) on average were smaller, with a smaller maximum clone size, than the denervated nail organ (Fig. 3*K*; mean cells/clone, 16.68; range of cells/clone, 1–98; $n = 53$), indicating that the observed pattern defects in bone after denervation and amputation include cell division differences by the respective clone forming cells.

To get a better mechanistic insight into the patterning defects observed in denervated and regenerating digits, we compared the relative levels of apoptosis by immunostaining for active caspase 3 protein at 2 wk postamputation and regeneration. Levels of caspase 3 immunostaining were very low in control (Fig. S4 *A* and *B*) and denervated (Fig. S4 *C* and D) tissues examined at 2 wk, with comparable levels detected in both groups (Fig. S4*E*). These results cumulatively indicate that apoptosis, an important cellular aspect of tissue replacement, is not dependent on nerve supply, despite phenotypes in epidermis, nail matrix, and bone/mesenchyme after denervation.

Nerve Dependence on Hind Limb Dermal Wound Healing. Humans heal full-thickness wounds primarily via granulation tissue formation and epidermal proliferation, whereas mouse wound healing involves epidermal proliferation and skin contraction (31). To investigate the possible effect of denervation on reepithelialization during wound healing, we used splinting of a rubber washer around a full-thickness 6-mm excisional wound with 8 symmetrically placed sutures (31). By splinting the wound, skin contraction is inhibited. Wound healing depends on epithelialization and cellular proliferation, which closely mirror the biological processes of human wound healing. To provide adequate denervated surface area on the upper limb for this wound healing model, in addition to surgical denervation of the sciatic and femoral nerves, we used a mouse model of SCI by unilateral transection of the spinal cord from T10-L4 (32). Two weeks after SCI, full-thickness splinted excisional wounds were performed and imaged for 14 d ($n = 7$). Wounds were then collected for histological analysis of epithelial and dermal layers, scar formation, and clonal tracing within the wound epidermis.

Histological analysis of wounds was carried out by analysis of hematoxylin and eosin and trichrome stains of 8-μM paraffin sections. Sections were analyzed throughout the entire wound regions. After 14 d of healing, wounds displayed similar epidermal thickness, intermediate replacement dermis that lacked in hair follicles, and distinct papillary dermis in the area of the wound, with dense connective tissue in the reticular dermis in control (Fig. 4 *A* and *C*; $n = 7$) and denervated (Fig. 4 *B* and *D*; $n = 7$) groups. In addition, hyperproliferation of keratinocytes was similarly detected in both groups, with mildly thickened cornified layers. Wounds of both groups displayed a similar inflammatory cell infiltrate in the dermis (observations by A.J.C.).

Reepithelialization of wounds, measured by normalizing the open wound area to the constant area within the inside of the rubber washer used for stinting (Fig. 4 *E* and *F*), indicated no significant difference in the rate of reepithelialization over the course of 2 wk between control and denervated groups (Fig. 4*G*). After wound closure, we performed clonal analysis of basal keratinocytes of the regenerated epidermis. Clones spanned basal keratinocyte and corneal layers of the epidermis, indicating continuous self-renewal and differentiation of epidermal progenitors in control (Fig. 4*H*; mean cells/clone, 4.71; range of cells/clone, 1–27; $n = 114$) and denervated (Fig. 4*I*; mean cells/clone, 5.48; range of cells/clone, 1–24; $n = 120$) repaired wound areas independent of the presence of hair follicles. These data indicate that reepithelialization during splinted excisional wound healing is independent of nerve and nerve-derived factors.

Discussion

An abundance of data across several vertebrate taxon groups (3, 11, 12) suggests that nerves may have a conserved evolutionary role that is essential to, or permissive for, limb regeneration. Despite the absence of innervation to the hind limb throughout the time of regeneration, the mouse model replaces the amputated digit

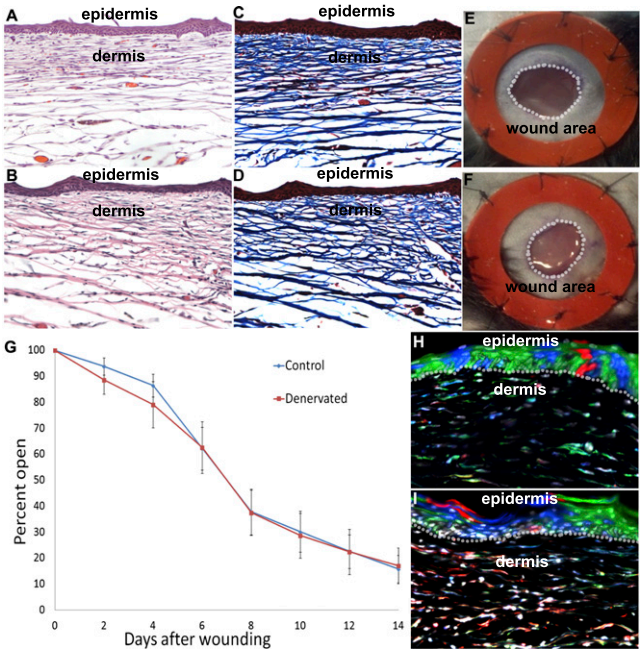

Fig. 4. Wound healing. Hematoxylin/eosin and trichrome histological stains of control (*A* and *C*) and denervated (*B* and *D*) cutaneous wounds display similar thickness, intermediate density replacement dermis, and hyperkeratosis in the area of the wound, and a mildly thickened cornified layer. Six-millimeter full-thickness stinted excisional wounds in control (*E*) and denervated (*F*) limbs close by reepithelialization (similar to human wound healing) with similar time courses (*G*). Clonal expansions in replacement epidermis span basal and corneal layers in control (*H*) and denervated (*I*) excisional wounds, indicating continuous renewal of basal keratinocyte layers and differentiation of keratinocytes into corneal layers after wound healing.

tip with surprising fidelity in most tissue types. Our comprehensive examination at single-cell levels of primary hind limb tissues during normal maintenance, regeneration, and wound healing reveals that many presumed tissue stem/progenitor cells maintain clonal and differentiation capabilities in the absence of nerve supply.

In salamander embryos, removal of a large section of the neural tube leads to limb development without innervation. These limbs can be transplanted to the flank of a normal larva, where they can regenerate in the absence of nerve supply (33). This lack of nerve dependence is made possible by the substitution of nerve-derived factors from ectodermal appendages, including epidermis and glands (33). In mice, a similar requirement for bone growth by ectodermal appendages is observed. Removal of the nail organ from the distal tips of mice leads to diminished growth of the distal phalanx bone (34) in a process mediated by Wnt signaling from the nail epithelium (20). Absence of Wnt signaling from the nail epithelium leads to diminished innervation after amputation and to subsequent inhibition of bone growth (20). It may be that absence of bone patterning in denervated and regenerated digits is an indirect effect of nerves on bones via nail epithelium, perhaps mediated by stromal cell-derived factor 1 (SDF1)/chemokine (C-X-C motif) receptor 4 (CXCR4) signaling in the distal phalanx. A similar regeneration defect of distal bone can be observed in transgenic mice devoid of SDF1/CXCR4 signaling (35), which could mechanistically explain the patterning defects observed in our murine denervation model (35).

Our findings of morphological defects in regenerating distal phalanx bone and nail matrix on denervation indicate that nerves affect tissue patterning in the distal extremities in both ectoderm- and mesoderm-derived tissues. Interestingly, these nerve-dependent phenomena bear similarities to human clinical and histopathological reports detailing patterning defects in the ectodermal and mesodermal tissue of SCI patients (17, 18).

In the denervated and regenerated nail matrixes, we find increased maximum clone size, fewer nondividing cells, and an overall increase in the number of cells per clone. This finding is particularly interesting considering the striking parallel to human clinical reports of nail hypertrophy in patients with SCI. In addition, regenerated digit tips in denervated limbs displayed accumulation of loose mesenchymal tissue and dense bundles of vascularization surrounding disorganized osseous bone in the denervated digit tips, rather than the trabecular osseous bone observed in control replacement digit tips. This disorganization results in an expanded size and abnormal appearance of the replacement digit tips reminiscent of nail hypertrophy and dermal fibrosis reported in SCI patients.

In addition, many patients in the SCI studies were also found to have significantly thickened skin on their lower limbs. Clonal analysis in keratinocytes and histology analysis on cutaneous wound healing showed that epidermal stem cells maintain function after denervation; however, these analyses did not reveal a significant difference in the thickness or quality of regenerated skin on the hind limb of control and denervated animals. The reports of skin thickening in SCI patients was found to be increased with severity and time after injury and could be explained by anatomic differences in skin architecture that are observed between mouse and humans. Perhaps the negative regulation of skin thickness is lost in denervated hind limbs.

Collectively, the nerve dependence of tissue replacement in the mouse hind limb bears resemblance to the complete dependence on nerves in adult amphibian regeneration and closely mirrors human SCI phenotypes. It seems probable, therefore, that SCI phenotypes may reflect underlying pathophysiology in mouse models and that medical treatment of these patients and translational medicine may benefit from further molecular studies into the nerve and nerve-factor regulation of hind limb tissues. For example, the translational implications of this study relate to the clinical problems seen with SCI patients involving both skin and bone. SCI patients develop skin thickening and chronic wounds (i.e., pressure ulcers), which represent a large medical burden. By understanding the mechanism or mechanisms of skin homeostasis with and without innervation, we may identify factors that can be used to prevent skin complications in SCI patients. Second, by understanding the mechanism or mechanisms through which innervation contributes to bone repair and patterning, we may identify factors that can be used to stimulate bone repair and patterning in SCI patients.

Experimental Procedures

Mice. Rainbow mice have been described previously (16) for clonal lineage tracing of individual cells. This reporter strain contains a multicolor Cre-dependent reporter construct in the ROSA locus ($R26^{VT2/GK3}$) and was crossed with mice containing an inducible Cre transgene under the ubiquitous Actin promoter ($Actin^{CreER}$). $Actin^{CreER}$; $R26^{VT2/GK3}$ (i.e. Rainbow) offspring were injected with 5 mg tamoxifen to activate single-cell fluorescent marking at the time of surgical amputation. Thus, on activation of Cre by tamoxifen injection, individual cells randomly and permanently express one of four fluorescent colors, allowing clonal expansion to be visualized as continuous regions of single colors. Wild-type animals were purchased from Jackson Laboratories. All animal procedures were carried out under the guidance of the Stanford University Administrative Panel on Laboratory Animal Care, protocol 21621.

Mice Genotyping. The following primers and PCR conditions were used for genotyping: Cre: CGGTCGATGCAACGAGTGATGAGG and CCAGAGACGGAAATCCATCGCTCG, 94 °C for 3 min, 94 °C for 30 s, 56 °C for 60 s, 72 °C for 60 s, repeat 35 cycles, 72 °C for 2 min.

Tamoxifen Injections. Tamoxifen (Sigma- Aldridge) was prepared in corn oil at 20 mg/mL, and 4–6mg doses were injected into the i.p. region.

Surgical Procedures. Femoral nerve branches innervate cutaneous tissues of the leg and foot, as well as ligaments, joints, and blood vessels. We therefore wanted to make sure complete denervation on hind limb tissues took place and that femoral nerve supply does not substitute sciatic nerve requirements (electrically, chemically, or functionally) after their denervation. Therefore, surgical denervation of both sciatic and femoral nerves was performed 2 wk before digit tip amputations to allow full Wallerian degeneration to take place. Although ablation of sciatic innervation alone denervates the distal limb, femoral ablation was performed to ensure no nerve regeneration from the proximal limb would occur during the regeneration time interval. An incision was made in the skin of the dorsal thigh, and the posterior muscles were divided to show the sciatic nerve. Sciatic denervation was achieved by cutting a 5-mm section of the sciatic nerve and cauterizing the proximal end of the nerve with bipolar forceps.

In addition, an incision was made in the ventral skin of the thigh and the femoral fascial sheath. Femoral denervation was achieved by cutting a 5-mm section of the femoral nerve, leaving the femoral artery intact. Sham surgeries were performed by exposing the nerves and closing the incision.

Surgical denervation of the upper limb/flank was performed 2 wk before full-thickness incisional wounds. An incision was made in the dorsal skin of the lower back, the tendons were divided to expose the spinal column, and a partial laminectomy was performed at the level of T12. Denervation was obtained by transection the right side of L1 spinal cord with a sharp microscalpel. Sham surgeries were performed by exposing the spinal cord.

Digit tip amputations were performed on digits 2–5 along the proximal third of the nail bed, as described previously (16).

Full-thickness excisional wounds 6 mm in diameter were created in pairs on the upper hind limb of the mouse. The skin and underlying panniculus were removed from the biopsy area. After the punch biopsy, rubber washers ~8 mm in diameter in their center are sutured in place around the wound to splint the wound open, preventing wound contracture allowing the formation of granulation tissue.

Histology and Histological Stains. For fixation, limb samples were placed in 2% (vol/vol) paraformaldehyde for 16 h at 4 °C and then prepared for embedding by soaking in 30% (vol/vol) sucrose in PBS at 4 °C for 24 h. Samples were removed from the sucrose solution and tissue blocks were prepared by embedding in Tissue Tek O.C.T (Sakura Finetek). Frozen blocks were mounted on a MicroM HM550 cryostat (MICROM International GmbH) and 8-μm-thick sections were transferred to Superfrost/Plus adhesive slides (Fisher).

Hematoxylin and eosin stains used Gill's hematoxylin to stain nuclei and acidified eosin to counterstain cytoplasm. Trichrome stains were performed according to Masson's method, with fixation in Boiun's solution, Wiegert's iron hematoxylin to stain nuclei, Biebrich scarlet-acid fuchsin to stain cytoplasm and keratin, and aniline blue to stain collagen fibers.

Morphometric Analysis. Digit samples from denervated (n = 3) and sham operated (n = 3) mice were sectioned serially from medial to lateral, and the midline section was used for all morphometry for each of eight control and eight denervated digits. The rate of taper was determined by tracing the outlines of the regenerated distal phalanges from digital images and by a best-fit slope of phalanx bone diameter compared with distance from the joint. The portions of outer bone that had undergone maturation to cortical bone were identified as being covered by periosteum and having no overlying osteoblasts or osteocytes. The percentage of the outer bone that had matured was assessed on the midline digital images.

Immunohistochemistry. Immunostaining was performed using Beta III tubulin (Abcam) and Cytokeratin 14 (Covance) primary antibodies and Alexa Fluor (Molecular Probes, Inc.) conjugated secondary antibodies.

Briefly, slides were blocked for 30 min in 5% (vol/vol) goat serum in PBS, followed by incubation with primary antibody for 12–16 h. For immunoassaying on sections from $Actin^{CreER}$; $R26^{VT2/GK3}$ mice, Alexa Fluor 647 conjugated antibody was used as secondary 1:1,000 for 1 h (Invitrogen) and was visualized in the far-red channel (Cy5). Fluorescent and bright-field images were taken with a Leica DM4000B microscope (Leica Microsystems) and RETIGA 2000R camera (QImaging Scientific Cameras).

Statistical Analysis. Hair follicle phase progression data were analyzed with a paired t test, using a Benjamini-Hochberg correction for multiple hypothesis testing.

1. Mizell M (1968) Limb regeneration: Induction in the newborn opossum. *Science* 161(3838):283–286.
2. Singer M (1952) The influence of the nerve in regeneration of the amphibian extremity. *Q Rev Biol* 27(2):169–200.
3. Singer M (1947) The nervous system and regeneration of the forelimb of adult Triturus; the relation between number of nerve fibers and surface area of amputation. *J Exp Zool* 104(2):251–265.
4. Birnie JH (1947) Regeneration and transplantation of fin rays in the goldfish. *Anat Rec* 99(4):648.
5. Singer M (1951) Introduction of regeneration of forelimb of the frog by augmentation of the nerve supply. *Proc Soc Exp Biol Med* 76(3):413–416.
6. Kumar A, Godwin JW, Gates PB, Garza-Garcia AA, Brockes JP (2007) Molecular basis for the nerve dependence of limb regeneration in an adult vertebrate. *Science* 318(5851):772–777.
7. Kumar A, Brockes JP (2012) Nerve dependence in tissue, organ, and appendage regeneration. *Trends Neurosci* 35(11):691–699.
8. Mullen LM, Bryant SV, Torok MA, Blumberg B, Gardiner DM (1996) Nerve dependency of regeneration: The role of Distal-less and FGF signaling in amphibian limb regeneration. *Development* 122(11):3487–3497.
9. Singer M (1974) Trophic functions of the neuron. VI. Other trophic systems. Neurotrophic control of limb regeneration in the newt. *Ann N Y Acad Sci* 228(0):308–322.
10. Stocum DL (2011) The role of peripheral nerves in urodele limb regeneration. *Eur J Neurosci* 34(6):908–916.
11. Geraudie J, Singer M (1977) Relation between nerve fiber number and pectoral fin regeneration in the teleost. *J Exp Zool* 199(1):1–8.
12. Singer M (1947) The nervous system and regeneration of the forelimb of adult Triturus; a further study of the importance of nerve number, including quantitative measurements of limb innervation. *J Exp Zool* 104(2):223–249.
13. Tu S, Johnson SL (2011) Fate restriction in the growing and regenerating zebrafish fin. *Dev Cell* 20(5):725–732.
14. Kragl M, et al. (2009) Cells keep a memory of their tissue origin during axolotl limb regeneration. *Nature* 460(7251):60–65.
15. Lehoczky JA, Robert B, Tabin CJ (2011) Mouse digit tip regeneration is mediated by fate-restricted progenitor cells. *Proc Natl Acad Sci USA* 108(51):20609–20614.
16. Rinkevich Y, Lindau P, Ueno H, Longaker MT, Weissman IL (2011) Germ-layer and lineage-restricted stem/progenitors regenerate the mouse digit tip. *Nature* 476(7361):409–413.
17. Stover SL, Hale AM, Buell AB (1994) Skin complications other than pressure ulcers following spinal cord injury. *Arch Phys Med Rehabil* 75(9):987–993.
18. Stover SL, Omura EF, Buell AB (1994) Clinical skin thickening following spinal cord injury studied by histopathology. *J Am Paraplegia Soc* 17(2):44–49.
19. Mohammad KS, Neufeld DA (2000) Denervation retards but does not prevent toetip regeneration. *Wound Repair Regen* 8(4):277–281.
20. Takeo M, et al. (2013) Wnt activation in nail epithelium couples nail growth to digit regeneration. *Nature* 499(7457):228–232.
21. Woo WM, Oro AE (2011) SnapShot: Hair follicle stem cells. *Cell* 146(2):334–e332, e2.
22. Schepers AG, et al. (2012) Lineage tracing reveals Lgr5+ stem cell activity in mouse intestinal adenomas. *Science* 337(6095):730–735.
23. Gupta V, Poss KD (2012) Clonally dominant cardiomyocytes direct heart morphogenesis. *Nature* 484(7395):479–484.
24. Blanpain C, Fuchs E (2009) Epidermal homeostasis: A balancing act of stem cells in the skin. *Nat Rev Mol Cell Biol* 10(3):207–217.
25. Brownell I, Guevara E, Bai CB, Loomis CA, Joyner AL (2011) Nerve-derived sonic hedgehog defines a niche for hair follicle stem cells capable of becoming epidermal stem cells. *Cell Stem Cell* 8(5):552–565.
26. Harris WH, Heaney RP (1969) Skeletal renewal and metabolic bone disease. *N Engl J Med* 280(6):303–311.
27. Becton JL, Winkelmann RK, Lipscomb PR (1966) Innervation of human finger tendons as determined by histochemical techniques. *J Bone Joint Surg Am* 48(8):1519–1524.
28. Guidry G, Landis SC (1998) Target-dependent development of the vesicular acetylcholine transporter in rodent sweat gland innervation. *Dev Biol* 199(2):175–184.
29. Tian H, et al. (2000) Catecholamines are required for the acquisition of secretory responsiveness by sweat glands. *J Neurosci* 20(19):7362–7369.
30. Lu CP, et al. (2012) Identification of stem cell populations in sweat glands and ducts reveals roles in homeostasis and wound repair. *Cell* 150(1):136–150.
31. Galiano RD, Michaels J, 5th, Dobryansky M, Levine JP, Gurtner GC (2004) Quantitative and reproducible murine model of excisional wound healing. *Wound Repair Regen* 12(4):485–492.
32. Pan W, Zhang L, Liao J, Csernus B, Kastin AJ (2003) Selective increase in TNF alpha permeation across the blood-spinal cord barrier after SCI. *J Neuroimmunol* 134(1-2):111–117.
33. Kumar A, et al. (2011) The aneurogenic limb identifies developmental cell interactions underlying vertebrate limb regeneration. *Proc Natl Acad Sci USA* 108(33):13588–13593.
34. Zhao W, Neufeld DA (1995) Bone regrowth in young mice stimulated by nail organ. *J Exp Zool* 271(2):155–159.
35. Lee J, et al. (2013) SDF-1α/CXCR4 signaling mediates digit tip regeneration promoted by BMP-2. *Dev Biol* 382(1):98–109.